Materials Horizons

Accepted Manuscript

This article can be cited before page numbers have been issued, to do this please use: H. Shang, X. Le, Y. Sun, S. Wu, Y. Wang, P. Theato and T. Chen, *Mater. Horiz.*, 2024, DOI: 10.1039/D4MH00210E.

ROYAL SOCIETY OF CHEMISTRY

rsc.li/materials-horizons

View Article Online
DOI: 10.1039/D4MH00210E

New concepts

The rapid advancement of technology has fueled a heightened demand for anti-counterfeiting labels, prompting the need for efficient methods in high-security label production. This study focuses on the development of advanced encryption labels capable of decoding and authenticating encoded information. It explores water-responsive multicolor fluorescent microgel systems, formed by combining microgels with cationic fluorescent dyes like FITC and Rh B. Synthesized from NIPAM, AAc, and 9-ANA, these microgels expand rapidly in water, altering fluorescence colors. Leveraging this, multi-color anti-counterfeiting labels are created using inkjet printing, revealing concealed information under UV light and undergoing water-based authentication. This research provides a robust methodology for crafting secure, easily decipherable anti-counterfeiting materials to meet the evolving needs of authentication in a technologically driven landscape.

View Article Online
DOI: 10.1039/D4MH00210E

ARTICLE

Water-sensitive fluorescent microgel inks to produce verifiable information for highly secured anti-counterfeiting

Received 00th January 20xx,
Accepted 00th January 20xx

DOI: 10.1039/x0xx00000x

Hui Shang,[a,b] Xiaoxia Le, [a,b,*] Yu Sun, [a,b] Shuangshuang Wu, [a,b] Yu Wang, [c] Patrick Théato [d] and Tao Chen [a,b,e,*]

The decryption and verification of encrypted information via a simple and efficient method is always difficult and challenging in the field of information security. Herein, a series of water-sensitive fluorescent microgels are fabricated for highly secured anti-counterfeiting with authenticity identification. The initial negatively charged microgels (MG) are made up of N-isopropylacrylamide (NIPAM), acrylic acid (AAc) and anthracen-9-yl acrylate (9-ANA, blue fluorescent monomer). The prepared MGs can bind cationic fluorescent dyes such as 5-aminofluorescein (FITC, green fluorescent dye) and Rhodamine B (Rh B, red fluorescent dye) via electrostatic interaction, emitting multi-fluorescent colors based on the fluorescence resonance energy transfer (FRET) process. Furthermore, the fluorescence colors of MG-derived systems can be rapidly changed by swelling in water, which can block the FRET process and change the aggregation state of dyes. With the assistance of inkjet printing, multi-color security patterns can be designed and encoded, which can be revealed by UV irradiation and further verified by water stimulation. This study has pioneered a novel strategy to verify the authenticity of decrypted information, which greatly improves the security level of information.

Introduction

The rapid development of science and technology has brought convenience for our life, also provided an opportunity for criminals to seek profits by making false information or commodities. The appearance of anti-counterfeiting labels has effectively reduced the occurrence of such incidents to a certain extent.[1-5] Nevertheless, common commercial security labels are generally manufactured through established procedures or methods, their high predictability and low security have led to the emergence of corresponding fake anti-counterfeiting labels. Therefore, it is urgent to develop new anti-counterfeiting materials and adopt cutting-edge anti-counterfeiting techniques.[6-12]

Fluorescent anti-counterfeiting labels have attracted wide attention due to the characteristic of fluorescence color concealment, which means it can only be displayed under a specific excitation wavelength.[13-19] For instance, Wu and colleagues[10] encoded multiple fluorescent patterns on a shape memory hydrogel, and the hidden information could only be decrypted under UV irradiation after shape recovery. Wang and coworkers[20] combined an oxygen-sensitive probe with oxygen permeable polymer matrix to achieve high security of multilevel information. The concealed message could only be visible when exposed to a certain concentration of oxygen under UV light. Unlike conventional fluorescent anti-counterfeiting strategies, these elegant attempts can improve the security of the message by adding decryption procedures. However, they are unable to eradicate the trouble caused by the imitation of fluorophores with similar colors.[7, 21-23]

A security label with dynamic change of fluorescence color can make up for the inherent defects that static fluorescence brought.[24-28] Wang's team fabricated dual-mode anti-counterfeiting patterns by photo-responsive supramolecular polymers consisting of anthracene-endoperoxide and energy acceptor fluorescent molecules. The process of FRET could be subtly regulated by either gas-induced polymerization process or photo-triggered anthracene-peroxide-lactone conversion, resulting in high-contrast fluorescence variations in three separate states.[29] Previously, our group designed a urea-containing hydrogel for protecting multistage information, where a protonated fluorescent unit could coordinate with various metal ions to load fluorescent information. When exposed to urea solution, the hidden information could be quickly displayed and erased during the procedure.[30] Though the controllable dynamic fluorescence transformations has successfully been achieved, it is still a huge challenge to quickly and effectively identify the authenticity of decrypted information. Moreover, another difficulty encountered in dynamic coding of multicolor fluorescence patterns is how to improve the accuracy and complexity of loading information.

[a.] *Key Laboratory of Advanced Marine Materials, Ningbo Institute of Materials Technology and Engineering, Chinese Academy of Sciences, Ningbo 315201, China. E-mail: lexiaoxia@nimte.ac.cn; tao.chen@nimte.ac.cn.*
[b.] *School of Chemical Sciences, University of Chinese Academy of Sciences, 19A Yuquan Road, Beijing 100049, China.*
[c.] *Shanghai Yuking Water Soluble Material Tech Co., Ltd, Banxia Road, Shanghai 200120, China.*
[d.] *Soft Matter Synthesis Laboratory, Institute for Biological Interfaces III, Karlsruhe Institute of Technology, Hermann-von-Helmholtz-Platz 1, 76344 Eggenstein-Leopoldshafen (Germany) and Institute for Chemical Technology and Polymer Chemistry, Karlsruhe Institute of Technology, Engesser Str.18, 76131 Karlsruhe (Germany).*
[e.] *College of Material Chemistry and Chemical Engineering Key Laboratory of Organosilicon Chemistry and Material Technology Ministry of Education Hangzhou Normal University Hangzhou 311121, China.*
Electronic Supplementary Information (ESI) available: [details of any supplementary information available should be included here]. See DOI: 10.1039/x0xx00000x

View Article Online
DOI: 10.1039/D4MH00210E

As a class of stimulus-responsive gels,[13, 31-36] polymeric microgels have the advantages of designability in terms of fast responsiveness and printable sizes, which is expected to be used for fluorescent labels via inkjet printing technology. Specially, such microgels show a rapid response to water stimulation, accompanied with changes in volume/morphology. Herein, anionic microgels (MG) were constructed by copolymerization of N-isopropylacrylamide (NIPAM), acrylic acid (AAc) and anthracen-9-yl acrylate (9-ANA) (**Scheme 1A**), which displayed blue fluorescence and exhibited rapid and conspicuous volume changes in presence or absence of water (**Figure S1**). The conspicuous volume changes stemmed that robust hydrogen bonding between water molecules and polymer chains, which facilitated the swift expansion of the microgel upon exposure to water., thus achieving rapid response times. Moreover, the deprotonated MG microgels could bind various cationic fluorescent dyes by electrostatic interaction. As typical representatives of cationic dyes, Rhodamine B (Rh B, red dye) and protonated 5-aminofluorescein (FITC, green dye) were selected for obtaining MG-derived systems with multicolor fluorescence emission (**Scheme 1B**). The MG-derived systems showed excellent fluorescence discoloration ability upon water stimulation (**Scheme 1C**), which could block the FRET process between the anthracene groups and the cationic dyes. In the meanwhile, the fluorescent color could also be affected by the aggregation state of dyes, which changed during microgels swelling. The instant dynamic fluorescence color-changing ability gave microgels the potential as fluorescent anti-counterfeiting inks (**Scheme 1D**). Assisted by an inkjet printer, a large-area information could be encoded, which could be read upon exposure to UV light and further identified the authenticity by water stimulation (**Scheme 1E-1G**). This study is the first to achieve high security level by verifying the decrypted information, providing ideas for the development of novel anti-counterfeiting materials.

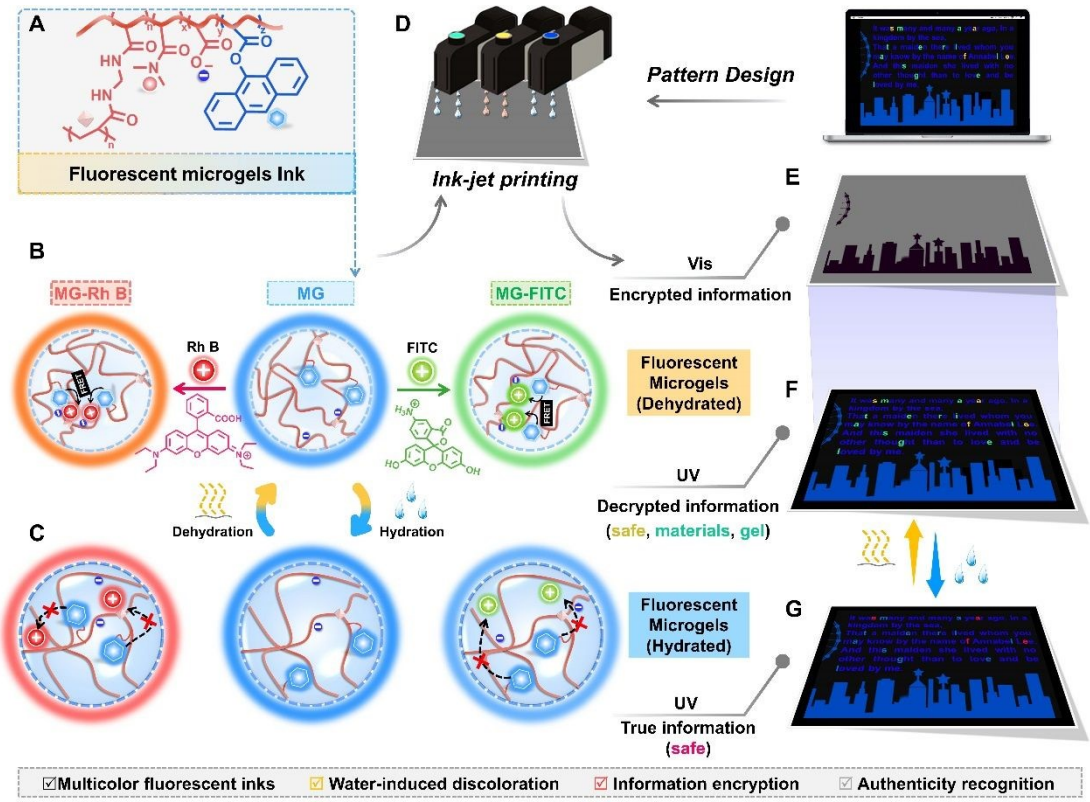

Scheme 1. Schematic illustration of multicolor fluorescent inks for information encryption. A) The chemical composition of fluorescent microgels inks. Microgel structures and the ensuing fluorescence color alterations within MG-derived microgels, comprising MG, MG-RhB, and MG-FITC, across dehydration B) and hydration C). D-G) The information printed with multicolor fluorescent inks, which can be displayed under UV light and verified by water stimulation.

Results and discussion

Synthesis and characterization of MG-derived systems

Poly(NIPAM-co-AAc-co-9-ANA) microgels (MG) were synthesized by a radical terpolymerization of NIPAM, AAc and 9-ANA (emitting blue fluorescence) via emulsion polymerization method (**Figure 1A**). ^{1}H Nuclear Magnetic Resonance (NMR) spectroscopy was conducted to reveal that 9-ANA has been successfully introduced into the microgel networks (**Figure 1B**). The prepared hydrated microgels with an average diameter of 155.8 nm (**Figure 1C**) exhibited negative charges (**Figure S2**), which provided anchoring points for the introduction of positive fluorescent dyes. In addition, SEM images (**Figure 1D**, **Figure S3**)

showed that the swollen microgels were perfectly spherical and homogeneous. Further, the microgels exhibited exceptional photophysical properties due to the existence of blue fluorescent emitter 9-ANA. As shown in **Figure 1E**, the MG solution displayed a blue fluorescence when excited at wavelengths ranging from 250 to 400 nm, especially at 254 nm (**Figure 1F**), which was also recorded by confocal laser scanning microscopy (CLSM) (**Figure 1G**). One thing that needs to be pointed out is that the particle size of the microgels significantly decreased to less than 100 nm after dehydration (**Figure S4**), which laid the foundation for the change of fluorescence colors. It could be preliminarily proved that the fluorescence intensity of MG is greatly weakened in the dry state (**Figure S5-S7**), which was caused by the aggregation-induced quenching (ACQ) effect of anthracene groups.

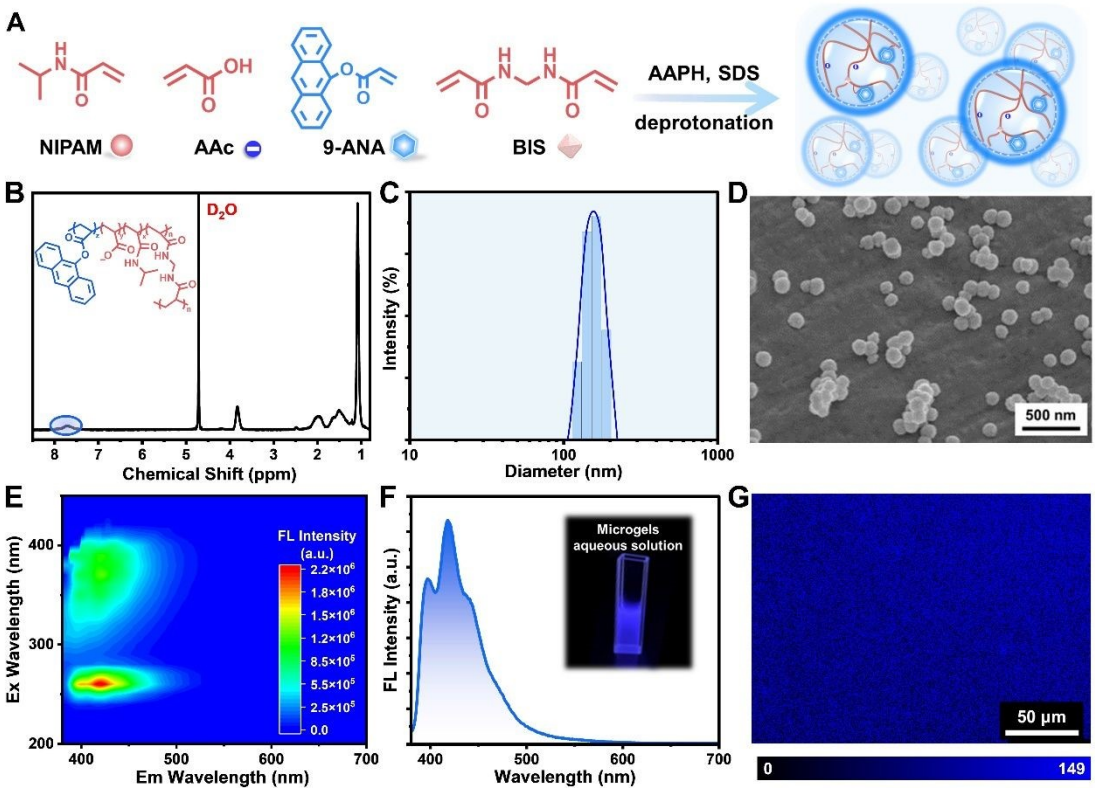

Figure 1. Morphology, composition and photophysical studies of prepared microgels. A) The synthesis routine of MG. B) 1H NMR spectrum of MG. C) DLS data and D) SEM image of MG. E) PL mapping spectra and F) Fluorescence spectra of MG solution. Insets: Photographs of the corresponding MG solution. G) CLSM image of MG.

Multicolor fluorescence emission based on MG-derived systems

MG containing negative-charged carboxylate functional groups could bind positive-charged fluorophores by electrostatic interaction, thus achieving multicolor fluorescence emission (**Figure 2A**). As two simple and easily available fluorescent dyes, Rhodamine B (Rh B) and 5-aminifluorescin (FITC) were selected because they are positively charged or easily protonated. Herein, the MG-derived systems, including MG-FITC (only adding FITC), MG-Rh B (only adding Rh B) and MG-1F1R (adding FITC and Rh B in a molar ratio of 1:1), were obtained by immersing pristine MG powder into a solution containing Rh B or FITC or both, before being dried. Following the incorporation of cationic dyes, the zeta potentials of the MG derivative systems are recorded as -0.5 mV (MG-FITC) and -3.1 mV (MG-Rh B) (**Figure S8**), which are higher than pure MG, indicating the successful anchoring of cationic dyes. Nevertheless, the introduction of cationic dyes does not have any effect on the microgels size (**Figure S9**), which are stable even after three months of storage (**Figure S10**). Additionally, it was feasible to verify the attachment of FITC and Rh B to the various MG-derived systems by utilizing an attenuated total reflection Fourier transformed infrared spectrometer (ATR-FTIR). As shown in **Figure 2B**, the spectra of MG-FITC, MG-1F1R and MG-Rh B showed several additional bands in comparison to that of pure MG. The stretching vibration of ring ethers had a developing absorption peak at 1340 cm^{-1} in the MG-FITC spectrum (green line). The five-membered cyclic lactone was responsible for creating the new peak at 1108 cm^{-1}. Besides, the spectrum of MG-Rh B (orange-red line) showed additional distinguishing bands at 1328 and 1261 cm^{-1}, which derived from the carboxylic acid group and aromatic ether in Rh B, respectively. Moreover, the bands at 1640 cm^{-1} of MG were shifted to 1633 cm^{-1} after the addition of FITC and Rh B, which

stemmed from electrostatic interaction between carboxylate and dyes. The emerging and alteration of these bands were all present in the spectrum of MG-1F1R (yellow line).

The introduction of fluorescent dyes had a great effect on the fluorescent properties of microgels. Compared with MG, the fluorescence intensity of other microgels systems significantly decreased at 380~480 nm as shown in the fluorescent spectra (**Figure 2C**). A singular fluorescence peak was detected at 530 nm for MG-FITC, and a prominent peak emerged at 590 nm in the case of MG-Rh B. Correspondingly, in the MG-1F1R system, two distinct peaks were apparent at 530 nm and 585 nm. It was possible that the whole networks contracted due to the electrostatic interactions between polymer chains and fluorescent dyes in the dry MG-derived systems, resulting in a fluorescence resonance energy transfer. This conjecture could be firstly confirmed by PL mapping spectra of the MG-derived systems. As depicted in **Figure 2D-2F**, the MG-derived systems showed a common feature that the intensity of the blue luminous center decreased and new luminous centers appeared.

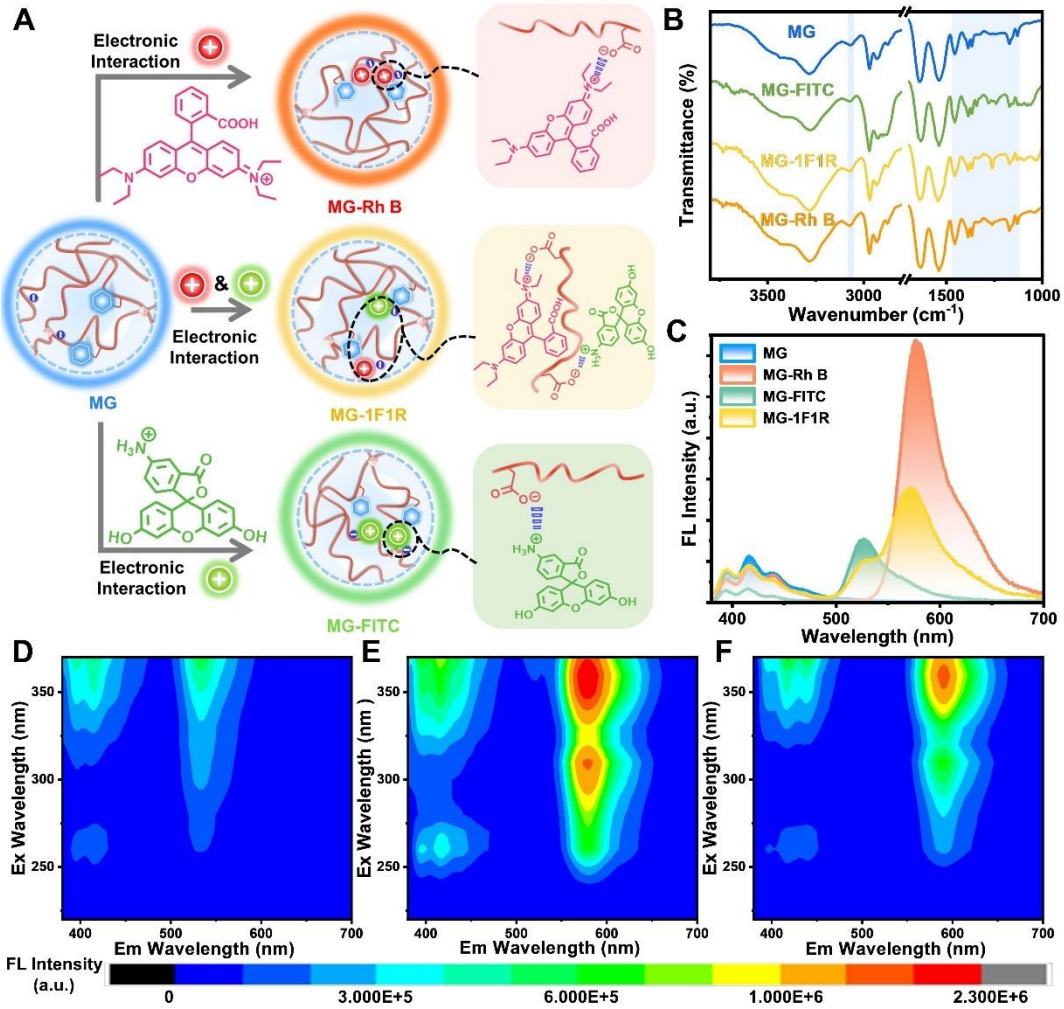

Figure 2. Multicolor fluorescence based on MG-derived systems. A) The diagrammatic drawing of multicolor microgels fabricated by adding positive-charged fluorescent dyes FITC, Rh B or both, respectively. B) ATR-FTIR spectra and C) fluorescent spectra of MG, MG-FITC, MG-1F1R and MG-Rh B. PL mapping spectra of MG-FITC (D), MG-1F1R (E) and MG-Rh B (F) powder at room temperature.

Water-induced fluorescence discoloration of MG-derived systems

Owing to the volume change of microgels during the swelling-deswelling process, the interaction between fluorescent dyes and polymer chains, as well as the distance between them and anthracene groups changed, leading to the variation of fluorescence color. Specifically, the MG-FITC sample emitted green fluorescence (530 nm) in its initial dry state. However, the fluorescence color changed to blue (415 nm) after water treatment, accompanied by a decrease in fluorescence intensity at 530 nm and an increase at 420 nm (**Figure 3A**). Relatively, other MG-derived systems, including MG-1F1R and MG-Rh B, also showed obvious red shifts of their fluorescent color before and after swelling in water (**Figure 3B** and **Figure 3C**). As can be seen in the CIE 1931 chromaticity diagram (**Figure 3D**), the various microgels exhibited obvious differences in color transformation. MG-FITC underwent a fluorescence transition from green to blue, and MG-Rh B exhibited a color

transformation from orange to red. Additionally, MG-1F1R similarly experienced a color alteration, changing from yellow to red. To verify the reversibility of discoloration process, fluorescence intensities of blue, green and red emission peaks were monitored. As shown in **Figure 3E**, there was no discernible decline in the fluorescence intensity and corresponding ratios of these microgels after six consecutive cycles of hydration-dehydration, which documented the outstanding reversibility of the fluorescence switch. This interesting phenomenon was possibly due to the synergistic effect of FRET and ACQ in the aggregation state and dispersion state of MG-derived systems (**Figure 3F-3G, Figure S11**). To be specific, the fluorescence emission intensity of Rh B can be enhanced due to the elimination of ACQ effect[37-39] when the microgels expanded in response to water stimulation, while the FRET effect between cationic dyes and anthracene units would be interrupted. Moreover, these microgel systems have impressive UV light stability even exposed to continuous UV light for 150 min (**Figure S12**).

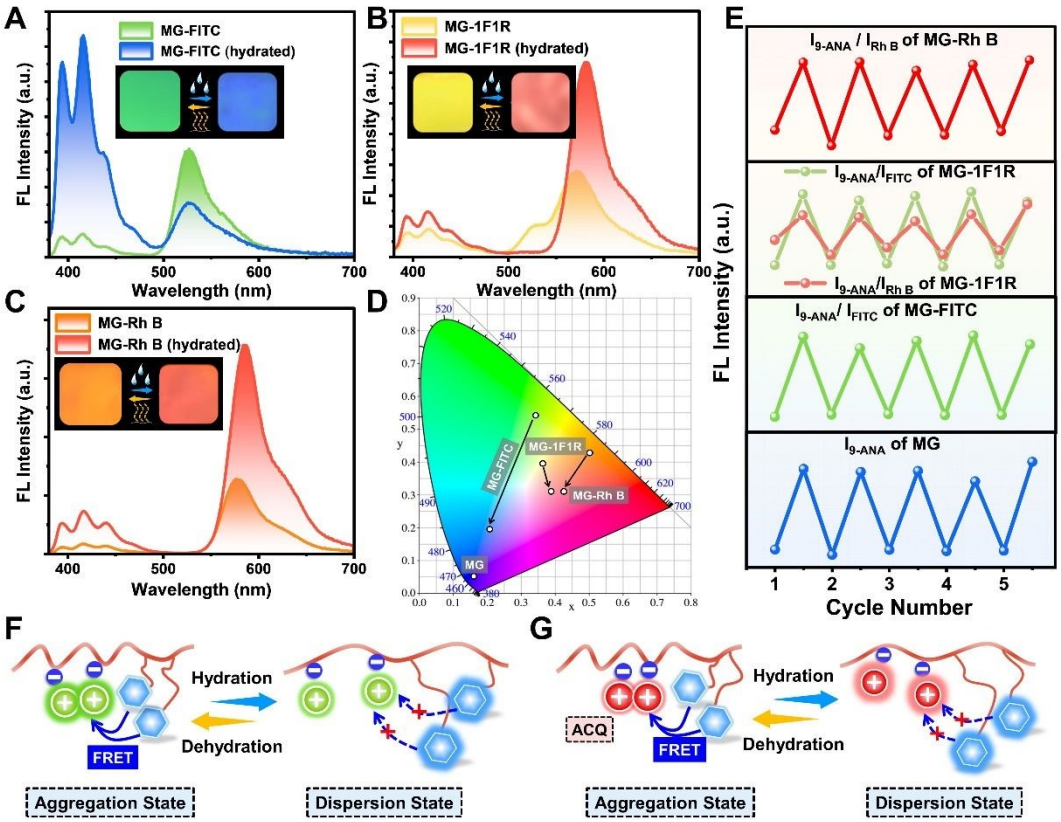

Figure 3. Water-triggered color variation of MG-derived systems. Fluorescent spectra of MG-FITC (A), MG-1F1R (B) and MG-Rh B (C) before and after treated with water. Insets: Corresponding photographs of the fluorescent color variation. D) The fluorescent color coordinates of MG, MG-FITC, MG-1F1R, MG-Rh B and their changes after treated with water in the CIE 1931 chromaticity diagram. E) The cyclic fluorescent changes of MG, MG-FITC, MG-1F1R and MG-Rh B during the sequential process of hydration and dehydration. F-G) The schematic diagram of the conjecture mechanism.

Mechanism of fluorescence discoloration in MG-derived systems

To better understand the mechanism of fluorescence discoloration, both experimental tests and theoretical simulations have been conducted. As shown in **Figure 4A**, pure MG displayed a broad emission peak in the blue region, spanning from 380 to 500 nm (λ_{ex} = 254 nm). By design, this emission spectrum precisely overlapped with the UV absorption spectra of both FITC (380~530 nm) and Rh B (380~600 nm), providing the potential occurrence of FRET. To test this hypothesis, the density functional theory (TD-DFT) calculations of conformation optimization, the highest occupied molecular orbital (HOMO) and lowest unoccupied molecular orbital (LUMO) electron densities of 9-ANA, FITC and Rh B were carried out.[40, 41] Compared with the HOMO-LUMO energy gap of 9-ANA (2.271 eV), FITC and Rh B had lower energy gaps calculated as 2.160 eV and 1.883 eV, indicating the possibility of electron transfer from anthracene moieties to cationic fluorescent dyes (FITC and Rh B) (**Figure 4B**). Furthermore, alterations in the fluorescence quantum efficiency and fluorescence lifetime concerning MG-FITC and MG-Rh B served as corroborative evidence for the occurrence of FRET process. In comparison to pure MG (**Figure 4C**), the fluorescence quantum efficiency of both MG-FITC and MG-Rh B exhibited a reduction within the wavelength range of 385~500 nm, declining from 20.82% to 7.93% and 7.17%, respectively. Conversely, within the range of

500~700 nm, there was a notable increase in fluorescence efficiency, rising from 3.17% to 17.85% for MG-FITC and a substantial enhancement to 67.28% for MG-Rh B, which signified an improvement in MG-derived systems without 9-ANA (**Figure S12-S13**). These results provided good evidence that the FRET process occurred. Nevertheless, the quantum efficiency of MG-FITC and MG-Rh B increased at the range of 385~500 nm and decreased at the range of 500~700 nm after water exposure. Especially, the quantum efficiency at 500~700 nm was not much different from that of hydrated MG-derived without 9-ANA, indicating that the FRET process was blocked. In addition, the fluorescence lifetime of MG-derived systems is also much longer than that of them without 9-ANA. Interestingly, hydrated MG-derived systems exhibit fluorescence lifetimes that were comparable to those observed in the absence of 9-ANA (**Figure S14-S15**), which highlights the role of hydration in modulating FRET. Pure MG (425 nm) maintains a nearly constant fluorescence lifetime (**Figure S16**), but the fluorescence lifetimes of MG-FITC (530 nm) and MG-Rh B (585 nm) decreased from 11.1 ns and 8.9 ns to 5.1 ns and 1.85 ns, respectively, when water was involved (**Figure 4D-4E**). These findings all demonstrated that the FRET process between energy acceptor (MG-FITC or MG-Rh

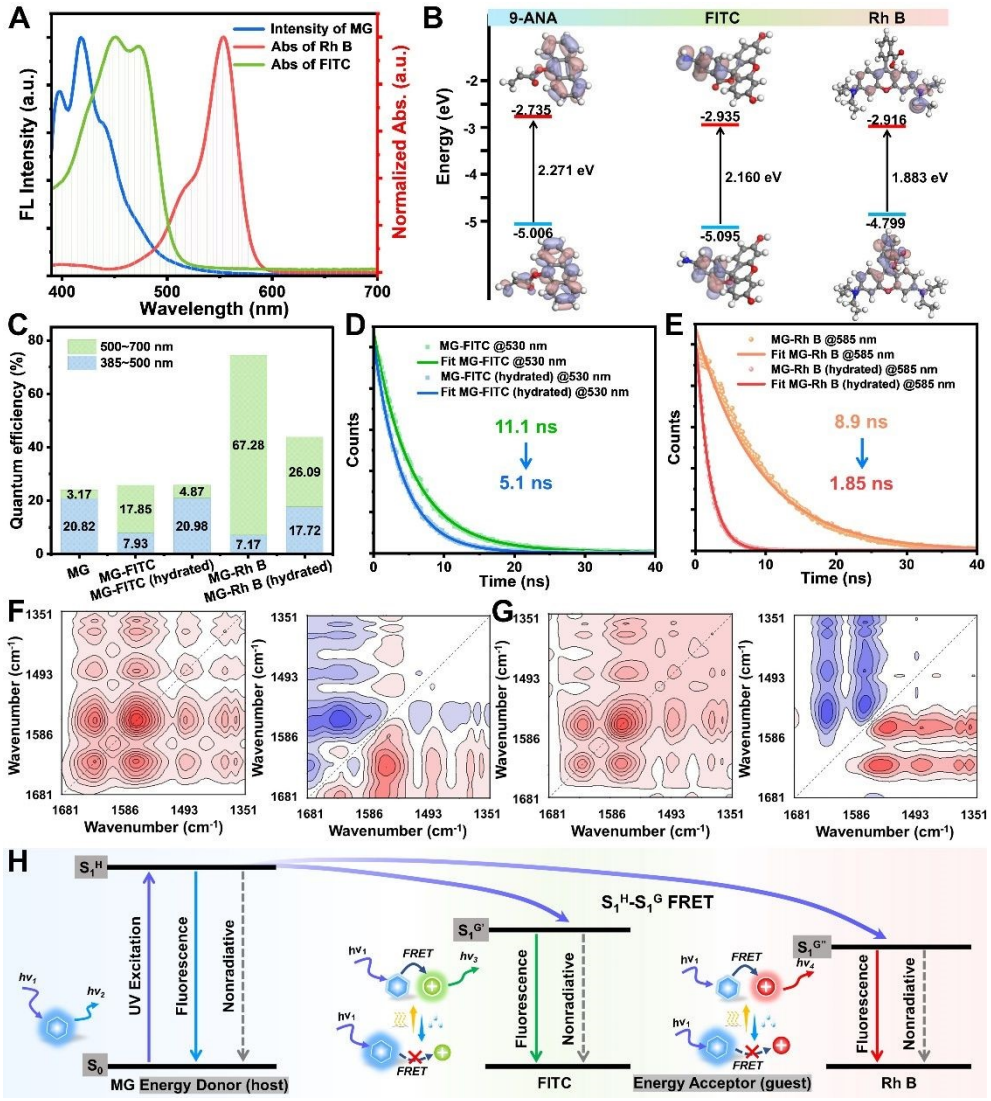

Figure 4. The mechanism of fluorescence discoloration in the MG-derived systems. A) The normalized UV absorption spectra of Rh B and FITC, and the fluorescence emission spectra of MG. B) LUMO and HOMO of structure-optimized 9-ANA, FITC and Rh B based on DFT calculations. C) The quantum efficiency of MG, and MG-FITC, MG-Rh B before and after water treatment in the 385~500 nm range and 500~700 nm range, respectively. D) The fluorescent lifetime of MG-FITC at 530 nm before and after water treatment. E) The fluorescent lifetime of MG-Rh B at 585 nm before and after water treatment. Two-dimensional COS synchronous spectra and asynchronous spectra generated from MG-FITC F) and MG-Rh B G) with different water content wherein red and blue colors are defined as positive and negative intensity, respectively. H) Mechanism of fluorescence processes in the MG-derived.

View Article Online DOI: 10.1039/D4MH00210F

To gain insight into the changes of chemical groups in MG-derived systems with or without water involved, FTIR spectroscopy was conducted. The peaks at 1385 and 1367 cm^{-1} were related to the methyl vibration of -$C(CH_3)_2$ in the polymer chains, the peak at 1640 cm^{-1} corresponded to the -COO^-, and the peak at 1539 cm^{-1} attributed to hydrogen bonds between C=O and N-H. Overall, the introduction of water molecules could cause the changes in the conformation of polymer chains and their interaction with fluorescent dyes (**Figure S17-S19**). To further analyze the dynamic process, ordinary FTIR spectra were converted to 2D correlation spectroscopy (2DCOS).[42, 43] The synchronous and asynchronous 2D-IR spectra of MG-FITC (**Figure 4F**) and MG-Rh B (**Figure 4G**) in the range of 1680–1350 cm^{-1} were recorded. The Φ (v_{1640}, v_{1539}), Φ (v_{1640}, v_{1385}) and Φ (v_{1640}, v_{1367}) in the synchronous spectrum and Ψ (v_{1640}, v_{1539}), Ψ (v_{1640}, v_{1385}), Ψ (v_{1640}, v_{1367}) in the asynchronous spectrum were positive and negative, respectively. According to Noda rule, the shifts of the peaks at 1539, 1385 and 1367 cm^{-1} were earlier than that at 1640 cm^{-1}, indicating that the swelling process of microgels precedes the dissolution of electrostatic interactions between molecular chains and fluorescent dyes. In other words, the FRET process would be gradually interrupted with the swelling of microgels.

Based on the analysis of above optical properties, the mechanism of FRET process between energy donor (9-ANA) and energy acceptor (FITC and Rh B) could be successfully documented, as shown in **Figure 4H**. During the FRET process, the majority of the photoexcited singlet excitons ($S1^H$) in the dry microgels matrix were transferred directly to the singlet excited state ($S1^G$), resulting in the radiating decay from $S1^G$ to the ground state and achieving efficient fluorescence emission. Meanwhile, the other part of the excitons ($S1^H$) emitted blue fluorescence in the form of radiative decay. Therefore, the dehydrated microgel entities exhibited a composite manifestation of diverse fluorescent hues, wherein MG corresponded to blue fluorescence, MG-FITC emitted a green fluorescence, and MG-Rh B was orange. When water was introduced, the FRET process from $S1^H$ to $S1^G$ was restricted, which enhanced blue emission and diminished green/red emission.

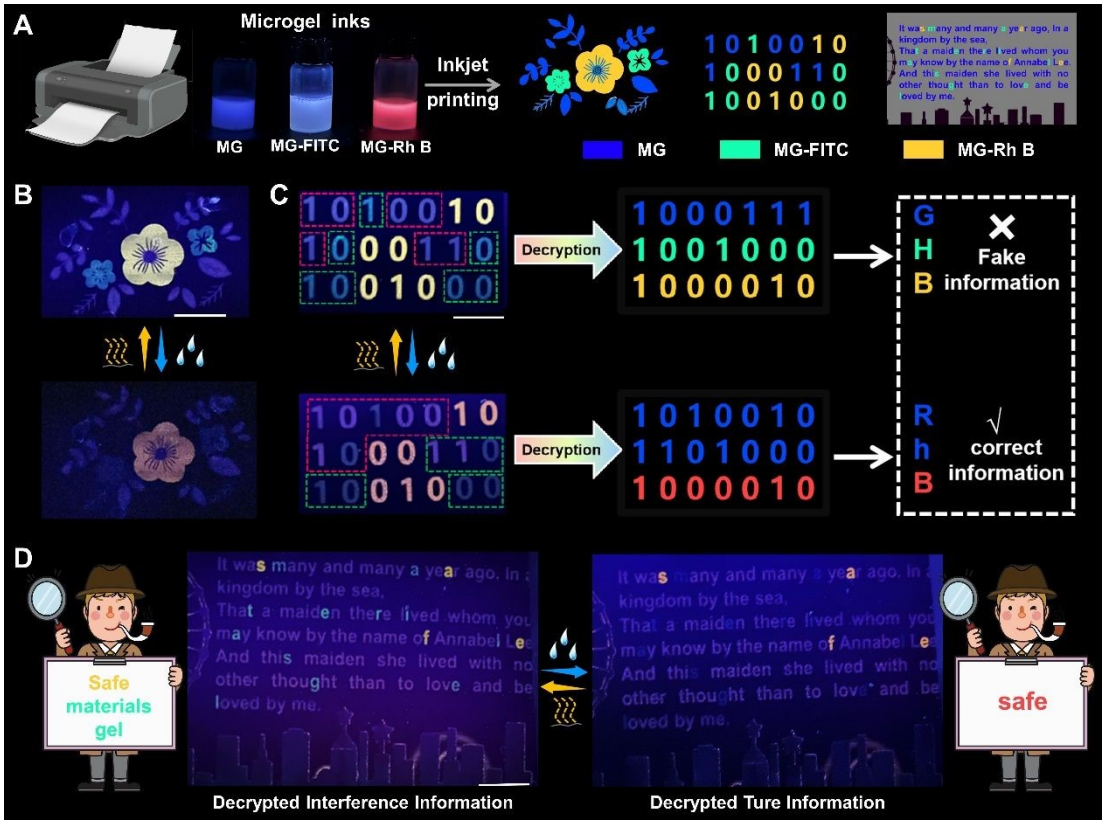

Figure 5. Inkjet printing of encrypted fluorescent patterns. A) Schematic diagram of inkjet printing process and programmed patterns printed by using fluorescent microgels (MG, MG-FITC and MG-Rh B) in three colors as inks. B) Photograph of the printed bouquet pattern before and after water stimulation under UV light of 254 nm. C) The printed multicolor binary codes can be decrypted into fake information and correct information, depending on presence or absence of water. D) Photograph of a paragraph printed by using tri-chromic fluorescent inks, respectively displaying words “safe, materials, gel” and “safe” before and after water stimulation under UV light of 254 nm (scale bar: 1 cm).

Anti-counterfeiting application of MG-derived systems

The fluorescent variation of microgels under water stimulation opens up a new way for advanced information encryption. Utilizing MG-derived systems as fluorescent inks, various information, including patterns, numbers, letters, could be written/printed with the assistance of a pen or an inkjet printer (**Figure S20** and **Figure 5A**). As a proof of concept, the printed bouquet demonstrated the capacity

for instantaneous alteration of its fluorescent coloration when subjected to water, with the ability to revert to its original state upon subsequent water evaporation (**Figure 5B**, **Movie S1**). Additionally, a series of binary code encryption tags was prepared using a method that integrated binary encoding with fluorescent colors as a cryptographic mechanism. Initially, the binary data was segmented based on fluorescent colors (blue, green, orange), and subsequently decrypted to reveal the hidden information as "GHB" (**Figure 5C, Movie S2**). Upon exposure to water stimulation, the fluorescent color corresponding to the information emerged, allowing the retrieval of the accurate information "Rh B" by arranging the same color codes in blue and red. This approach amalgamates fluorescent labeling with color coding, ensuring both concealment and the ability to decode through specific steps, thereby guaranteeing security and confidentiality. It's worth mentioning that the encryption-decryption process could be repeated for multiple cycles, ensuring the stability of stored information (**Figure S21**).

In the pursuit of enhancing security measures, the integration of commercial inks with microgel fluorescent inks was undertaken. Consequently, certain seemingly inconsequential patterns or messages printed with commercial inks remained discernible under visible light. However, the authentic content became visible under UV illumination or upon exposure to water. To illustrate, one could only see the window and the moon, clouds outside under natural light, but one could see the hidden QR code under the UV light (**Figure S22A**). Similarly, visible light revealed solely the presence of a tree trunk and branches, but UV light exposure unveiled yellow and green fruits. Furthermore, the red fruits became visible upon contact with water (**Figure S22B**). As depicted in **Figure 5D**, three words including "safe", "materials", "gel" could be discerned through color recognition in the poem when subjected to UV light. However, nothing but background was shown under visible light (**Figure S23**). When exposed to water stimulation, a single word, "safe", with altered coloration became apparent, thereby facilitating the differentiation between authentic and counterfeit information. As indicated above, these features give rise to a new encryption method, which can further improve the security level. It is worth noting that our fluorescent patterns can be stored for more than one year (**Figure S24**).

Conclusions

In summary, we have presented a series of printable microgels with fluorescence color-changing properties in response to water for highly secured anti-counterfeiting. The initial poly(NIPAM-co-AAc-co-9-ANA) microgel (MG) was fabricated by the copolymerization of NIPAM, AAc and 9-ANA (blue fluorescence emitter). Owing to the existence of carboxylic groups, MG can bond with cationic fluorescent dyes such as FITC and Rh B via electrostatic interaction, obtaining MG-derived systems called MG-FITC and MG-Rh B. These microgels exhibited multicolor fluorescence in dry state based on FRET between anthracene moieties and cationic fluorescent dyes. When exposed to water, the FRET process can be interrupted, and aggregation degree of Rh B is decreased, accompanied by remarkable fluorescent switches. Given the dramatic differences in fluorescent properties before and after water treatment, our microgels can serve as smart inks to print confidential information with the assistance of inkjet printing technology. The encoded information decrypted under UV irradiation can be rapidly verified by water stimulation. In a word, our strategy provides a new idea to decrypt hidden information with high security level in a simple way, which is expected to have potential applications in fields such as anti-counterfeiting labels.

Author Contributions

Hui Shang: Methodology, Data curation, Formal analysis, Investigation, Writing - original draft. Xiaoxia Le: Conceptualization, Formal analysis, Writing - review & editing, Supervision. Yu Sun: Data curation, Supervision Shuangshuang Wu: Data curation, Supervision. Yu Wang: Supervision. Patrick Théato: Writing - review & editing. Tao Chen: Supervision, Conceptualization.

Conflicts of interest

There are no conflicts to declare.

Acknowledgements

This work was supported by the National Key R&D Program of China (2022YFB3204300), the National Natural Science Foundation of China (52103246), Zhejiang Provincial Natural Science Foundation of China (LQ22E030015), Natural Science Foundation of Ningbo (2023J408, 20221JCGY010301), Ningbo International Cooperation Project (2023H019), and the Sino-German Mobility Program (M-0424).

Notes and references

1. R. Arppe and T. J. Sørensen, *Nat. Rev. Chem.*, 2017, **1**, 0031.
2. B. Berman, *Bus. Horiz.*, 2008, **51**, 191-199.
3. J. Liao, C. Ye, J. Guo, C. E. Garciamendez-Mijares, P. Agrawal, X. Kuang, J. O. Japo, Z. Wang, X. Mu, W. Li, T. Ching, L. S. Mille, C. Zhu, X. Zhang, Z. Gu and Y. S. Zhang, *Mater. Today*, 2022, **56**, 29-41.
4. M.-K. Tsang, G. Bai and J. Hao, *Chem. Soc. Rev.*, 2015, **44**, 1585-1607.
5. H. Zhang, D. Hua, C. Huang, S. K. Samal, R. Xiong, F. Sauvage, K. Braeckmans, K. Remaut and S. C. De Smedt, *Adv. Mater.*, 2020, **32**, e1905486.
6. Y. Gu, C. He, Y. Zhang, L. Lin, B. D. Thackray and J. Ye, *Nat. Commun.*, 2020, **11**, 516.
7. X. Ji, R. T. Wu, L. Long, X. S. Ke, C. Guo, Y. J. Ghang, V. M. Lynch, F. Huang and J. L. Sessler, *Adv. Mater.*, 2018, **30**, 1705480.
8. S. Liu, J. Wang, F. Tang, N. Wang, L. Li, C. Yao and L. Li, *ACS Appl. Mater. Interfaces*, 2020, **12**, 55269-55277.
9. H. Wang, X. Yin and L. Wang, *J. Mater. Chem. C*, 2018, **6**, 11569-11574.

10. C. N. Zhu, T. Bai, H. Wang, J. Ling, F. Huang, W. Hong, Q. Zheng and Z. L. Wu, *Adv. Mater.*, 2021, **33**, e2102023.
11. H. Deng, H. Wang, Y. Tian, Z. Lin, J. Cui and J. Chen, *Mater. Horiz.*, 2023, **10**, 5256-5262.
12. H. Wang, J. Tang, H. Deng, Y. Tian, Z. Lin, J. Cui and J. Chen, *J. Mater. Chem. C*, 2023, **11**, 15945-15951.
13. X. He, J. Zhang, X. Liu, Z. Jin, J. W. Y. Lam and B. Z. Tang, *Angew. Chem. Int. Ed.*, 2023, **62**, e202300353.
14. H. Im, J. Yoon, J. Choi, J. Kim, S. Baek, D. H. Park, W. Park and S. Kim, *Adv. Mater.*, 2021, **33**, e2102542.
15. X. Le, H. Shang, S. Wu, J. Zhang, M. Liu, Y. Zheng and T. Chen, *Adv. Funct. Mater.*, 2021, **31**, 2108365.
16. J. Liu, H. Rijckaert, M. Zeng, K. Haustraete, B. Laforce, L. Vincze, I. Van Driessche, A. M. Kaczmarek and R. Van Deun, *Adv. Funct. Mater.*, 2018, **28**, 1707365.
17. Y. Niu, X. Yang, J. Li, Y. Zeng, K. Liu, W. Wan, J. Liao, M. Wei, S. Li, J. Zhang, Z. Chong, X. Du and Z. Gu, *Mater. Today*, 2022, **57**, 57-65.
18. Y. Chen, H. Wang, X. Xu, H. Ye, C. Xiao, J. Bai, M. Xie, S. Chen, I. Jeon, D. Yu, T. Chen and X. Wu, *Chem. Eng. J.*, 2024, **488**, 150765.
19. X. Xu, C. Xiao, Y. Chen, D. Yu, Y. Lu, I. Wyman and X. Wu, *Green Chemical Engineering*, 2023, **4**, 379-386.
20. L. Ding and X.-d. Wang, *J. Am. Chem. Soc.*, 2020, **142**, 13558-13564.
21. H. Wang, X. Ji, Z. A. Page and J. L. Sessler, *Mater. Chem. Front.*, 2020, **4**, 1024-1039.
22. D. Zhou, D. Liu, W. Xu, X. Chen, Z. Yin, X. Bai, B. Dong, L. Xu and H. Song, *Chem. Mater.*, 2017, **29**, 6799-6809.
23. X. Li, H. Wang, J. Chen, Y. Tian, C. Xiang, W. Liu, Z. Zhou, J. Cui and X. Chen, *Adv. Funct. Mater.*, 2023, **33**, 2303765.
24. Z. Li, H. Chen, B. Li, Y. Xie, X. Gong, X. Liu, H. Li and Y. Zhao, *Adv. Sci.*, 2019, **6**, 1901529.
25. Z. Li, G. Wang, Y. Ye, B. Li, H. Li and B. Chen, *Angew. Chem. Int. Ed.*, 2019, **58**, 18025-18031.
26. P. Long, Y. Feng, C. Cao, Y. Li, J. Han, S. Li, C. Peng, Z. Li and W. Feng, *Adv. Funct. Mater.*, 2018, **28**, 1800791.
27. Q. Qi, C. Li, X. Liu, S. Jiang, Z. Xu, R. Lee, M. Zhu, B. Xu and W. Tian, *J. Am. Chem. Soc.*, 2017, **139**, 16036-16039.
28. S. Ye, N. Meftahi, I. Lyskov, T. Tian, R. Whitfield, S. Kumar, A. J. Christofferson, D. A. Winkler, C.-J. Shih, S. Russo, J.-C. Leroux and Y. Bao, *Chem*, 2023, **9**, 924-947.
29. Z. Gao, Y. Han and F. Wang, *Nat. Commun.*, 2018, **9**, 3977.
30. X. Le, H. Shang, H. Yan, J. Zhang, W. Lu, M. Liu, L. Wang, G. Lu, Q. Xue and T. Chen, *Angew. Chem. Int. Ed.*, 2020, **60**, 3640-3646.
31. L. Li, J. M. Scheiger, T. Tronser, C. Long, K. Demir, C. L. Wilson, M. A. Kuzina and P. A. Levkin, *Adv. Funct. Mater.*, 2019, **29**, 1902906.
32. J. Liu, Q. Guo, X. Zhang, J. Gai and C. Zhang, *Adv. Funct. Mater.*, 2021, **31**, 2106673.
33. M. Nie, C. Huang and X. Du, *Nanoscale*, 2021, **13**, 2780-2791.
34. Y. Sun, X. Le, S. Zhou and T. Chen, *Adv. Mater.*, 2022, **34**, 2201262.
35. H. Wang, Z. Liu, Z. Liu, J. Jiang and G. Li, *ACS Appl. Mater. Interfaces*, 2021, **13**, 59310-59319.
36. Q. Zhang, Y. Jiang, L. Chen, W. Chen, J. Li, Y. Cai, C. Ma, W. Xu, Y. Lu, X. Jia and Z. Bao, *Adv. Funct. Mater.*, 2021, **31**, 2100686.
37. W. Han, X. Zhang, M. Chen, X. Chu, W. Li, P. Fu, Z. Jia and Y. Li, *Dyes Pigm.*, 2023, **215**, 111244.
38. A. Kasparek and B. Smyk, *Acta A Mol. Biomol. Spectrosc.*, 2018, **198**, 297-303.
39. T. Xiong, Y. Zhang, N. Amin and J.-C. Tan, *Molecules*, 2021, **26**, 7583.
40. H. Su, K. Hu, W. Huang, T. Wang, X. Zhang, B. Chen, H. Miao, X. Zhang and G. Zhang, *Angew. Chem. Int. Ed.*, 2023, **62**, e202218712.
41. G. Sun, Y. C. Wei, Z. Zhang, J. A. Lin, Z. Y. Liu, W. Chen, J. Su, P. T. Chou and H. Tian, *Angew. Chem. Int. Ed.*, 2020, **59**, 18611-18618.
42. K. Gong, L. Hou and P. Wu, *Adv. Mater.*, 2022, **34**, e202201065.
43. H. Wang, H. Liu, Z. Cao, W. Li, X. Huang, Y. Zhu, F. Ling, H. Xu, Q. Wu, Y. Peng, B. Yang, R. Zhang, O. Kessler, G. Huang and J. Wu, *Proc. Natl. Acad. Sci.*, 2020, **117**, 11299-11305.

View Article Online DOI: 10.1039/D4MH00210E